

Evolution of Electronic States and Emergence of Superconductivity in the Polar Semiconductor GeTe by Doping Valence-Skipping Indium

M. Kriener^{1,*}, M. Sakano,² M. Kamitani,¹ M. S. Bahramy,^{1,2} R. Yukawa,³ K. Horiba,³
H. Kumigashira,^{3,4} K. Ishizaka,^{1,2} Y. Tokura,^{1,2,5} and Y. Taguchi¹

¹RIKEN Center for Emergent Matter Science (CEMS), Wako 351-0198, Japan

²Department of Applied Physics and Quantum-Phase Electronics Center (QPEC), University of Tokyo, Tokyo 113-8656, Japan

³Photon Factory, Institute of Materials Structure Science, High Energy Accelerator Research Organization (KEK), Tsukuba, Ibaraki 305-0801, Japan

⁴Institute of Multidisciplinary Research for Advanced Materials (IMRAM), Tohoku University, Sendai 980-8577, Japan

⁵Tokyo College, University of Tokyo, Tokyo 113-8656, Japan



(Received 5 April 2019; published 31 January 2020)

GeTe is a chemically simple IV–VI semiconductor which bears a rich plethora of different physical properties induced by doping and external stimuli. Here, we report a superconductor-semiconductor-superconductor transition controlled by finely-tuned In doping. Our results reveal the existence of a critical doping concentration $x_c = 0.12$ in $\text{Ge}_{1-x}\text{In}_x\text{Te}$, where various properties, including structure, resistivity, charge carrier type, and the density of states, take either an extremum or change their character. At the same time, we find indications of a change in the In-valence state from In^{3+} to In^{1+} with increasing x by core-level photoemission spectroscopy, suggesting that this system is a new promising playground to probe valence fluctuations and their possible impact on structural, electronic, and thermodynamic properties of their host.

DOI: 10.1103/PhysRevLett.124.047002

Superconductivity emerges from a wide range of parent materials, including insulators and semiconductors, e.g., by doping, pressurizing, photoirradiation, etc. When charge carriers are doped by partial substitution of one element for another to form out a sufficiently large density of states (DOS) at the Fermi level (E_F), superconductivity is established, provided that an effective attractive interaction works among electrons via lattice vibrations. Therefore, choosing appropriate dopant atoms offers to influence superconductivity through the formation of DOS at E_F , the provision of the attractive interaction among electrons, and the frequency of lattice vibrations. Historically, it was in the early 1960s that Cohen predicted superconductivity in many-valley semiconductors and semimetals [1] due to their peculiar band structure, which was experimentally confirmed soon after. Among them is SnTe, which exhibits superconductivity below critical temperatures T_c of less than 300 mK. Interestingly, T_c is strongly enhanced by In doping in its cubic structure [2–4]. To explain this, the valence-skipping nature [5–8] of In has been discussed [2–4], likewise Bi, Sn, and Tl. It should formally take its divalent state but is expected to form out, instead, In^{1+} and In^{3+} or a mixture of both. On the basis of the “negative- U mechanism” [5], the valence-skipping nature is predicted to enhance the superconducting interaction as discussed for Tl-doped PbTe [9], Ag-doped SnSe [10,11], and K-doped BaBiO₃ [12].

These interesting implications for superconductivity turned our attention to GeTe [13], which exhibits a rich variety of different phenomena [29], such as superconductivity [30],

structural phase change memory functionality [31] and its magnetic analogue [32,33], ferromagnetism, multiferroicity [34–36], and good thermoelectric properties [37] owing to its multivalley band structure [38]. Recently, it was pointed out that GeTe has potential to bear topologically nontrivial physics, making the system even more attractive [39]. It is also well known for a large Rashba spin splitting of its bulk bands due to strong spin-orbit coupling and a polar distortion [40–42] around 700 K from cubic to rhombohedral accompanied with an elongation of the unit cell along the cubic [111] direction, see Fig. 1(a) [45]. The band structure is shown in Fig. 1(b) for cubic GeTe. The valence band is mainly of Te $5p$ character while the conduction band primarily consists of Ge $4p$. Figure 1(c) gives a schematic view of the DOS (left [46]) and the approximate position of the atomic orbitals of In (right). In both panels, the small-gap feature of semiconducting GeTe is apparent. In reality, however, GeTe features a metalliclike resistivity and superconducts at $T_c \lesssim 300$ mK owing to unintentionally doped holes due to Ge deficiency ($\text{Ge}_{1-\delta}\text{Te}$) [47]. Thus far, there have been only a few reports available focusing on thermoelectric properties and structure in $\text{Ge}_{1-x}\text{In}_x\text{Te}$ and superconductivity in related systems [48–51].

In this Letter, we report the growth of $\text{Ge}_{1-x}\text{In}_x\text{Te}$ by employing a high-pressure synthesis method, the discovery of a doping-induced superconductor-semiconductor-superconductor transition, and the existence of a critical doping level ($x_c = 0.12$) by means of transport and specific-heat measurements. The results imply that a change of the

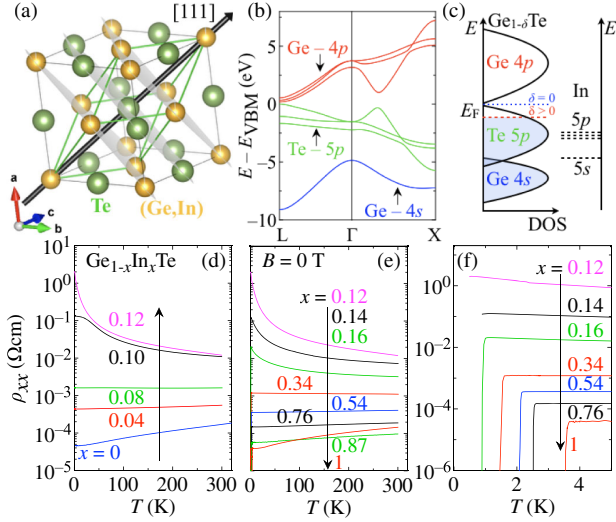


FIG. 1. (a) Schematic of the unit cell of GeTe. The grey cube denotes the high- T cubic unit cell, green the low- T rhombohedrally distorted modification. The black arrow indicates the cubic [111] direction along which the distortion takes place, cf. Ref. [32]. (b) Band structure of cubic GeTe. The direct band gap of ~ 0.2 eV is located at the L point of the Brillouin zone. The valence-band maximum (VBM) is set to be zero energy. (c) Sketch of the density of states for $\text{Ge}_{1-\delta}\text{Te}$ [46] and the atomic energy levels of the In dopant. The blue dotted line indicates E_F for ideal GeTe without Ge vacancies ($\delta = 0$). The more realistic case of $\text{Ge}_{1-\delta}\text{Te}$ is indicated with a red dashed line. Temperature-dependent resistivities $\rho_{xx}(T)$ of $\text{Ge}_{1-x}\text{In}_x\text{Te}$ for (d) $0 \leq x \leq x_c$ and (e) $x_c \leq x \leq 1$. (f) Expanded view of (e) for $T \leq 5$ K.

In-valence state from In^{3+} (electron doping) to In^{1+} (hole doping) plays a role. Core-level photoemission-spectroscopy (PES) data support this scenario: At higher doping additional features appear, indicating a different In-valence state. A model is proposed which explains satisfactorily all observed features. These results indicate that the valence-skipping feature of In governs, or is intimately coupled with, the structural and electronic properties, including the emergence of superconductivity, of the whole phase diagram. For the details of sample preparation, characterization, and measurements, see the Supplemental Material (SM) [14].

Temperature (T) dependent resistivities ρ_{xx} are summarized in Figs. 1(d) ($0 \leq x \leq 0.12$) and 1(e) ($0.12 \leq x \leq 1$). As for the $\text{Ge}_{1-\delta}\text{Te}$ sample used here, $\delta \approx 1.8\%$ is estimated from the charge-carrier concentration at 300 K, giving rise to metallic conduction [52]. When doping In, the absolute values of ρ_{xx} increase drastically. While $x = 0.04$ still exhibits a metalliclike T dependence, samples with $x \geq 0.1$ feature a semiconductorlike $\rho_{xx}(T)$. The largest absolute value of ρ_{xx} is found for $x_c = 0.12$. As compared to $x = 0$, ρ_{xx} at 2 K is enhanced by 5 orders of magnitude. Nevertheless, ρ_{xx} (with the order of a few Ω cm at 2K) exhibits a power-law T dependence being clearly distinct from activation type and, hence, cannot be associated with a finite band gap. Upon further increasing x , ρ_{xx} becomes

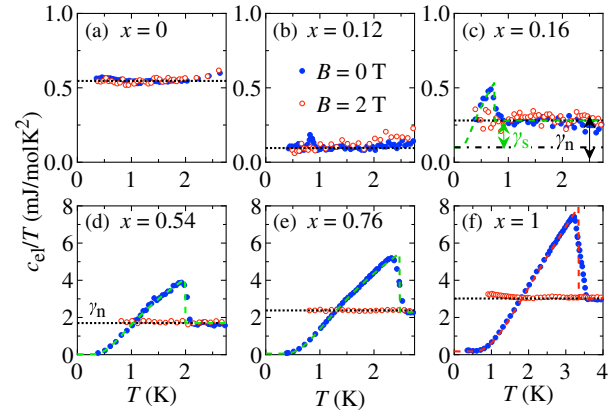


FIG. 2. Specific heat of $\text{Ge}_{1-x}\text{In}_x\text{Te}$ for selected x measured in $B = 0$ T (blue filled symbols) and $B = 2$ T (red open symbols), which is sufficient to suppress the superconductivity. Dotted black lines denote the normal-state electronic specific-heat coefficient γ_n , dashed lines denote the electronic specific heat in weak [green in (c)–(e)] or strong-coupling [red in (f)] BCS theory, see text. Specific-heat anomalies are observed for $x \geq 0.16$, indicating the formation of bulk superconductivity, which does not yet develop over the whole sample for $x = 0.16$ as indicated by a residual nonsuperconducting phase $\gamma_n - \gamma_s$.

again smaller, and for $x > 0.44$, all studied samples exhibit a metalliclike $\rho_{xx}(T)$. Figure 1(f) provides an expanded view for $T < 5$ K, revealing superconducting transitions as indicated by sharp drops in $\rho_{xx}(T)$ for $x \geq 0.16$. Moreover, T_c monotonically increases with x .

Electronic specific-heat data c_{el} of selected samples are displayed as c_{el}/T vs T plots in Fig. 2. For the details of the analyses, cf. Ref. [4]. In agreement with resistivity, there is no anomaly visible for $x = 0$ in the T range ≥ 350 mK [Fig. 2(a)]. Doping In leads to a suppression of the normal-state electronic specific-heat coefficient γ_n , and, hence, the DOS at E_F . The lowest γ_n value is found for $x_c = 0.12$ [Fig. 2(b)] which is most insulating. For $x = 0.16$ [Fig. 2(c)], there is a jumplike anomaly on top of a residual DOS corresponding to a nonsuperconducting phase fraction of $\sim 35\%$. Upon further doping, all samples are found to be bulk superconductors with vanishing or rather small residual DOSs. Moreover, the transitions are sharp, indicating a good sample quality. Up to $x = 0.87$, c_{el}/T data can be well reproduced by weak-coupling Bardeen-Cooper-Schrieffer (BCS) theory [Fig. 2(c)–2(e)] with $\Delta/k_B T_c = 1.764$ (Δ represents the superconducting gap). However, for $x = 1$, it is necessary to increase $\Delta/k_B T_c$ to 1.95 to yield a satisfactory description [Fig. 2(f)]. This apparent difference is discussed in Section S9 of the SM [14]. As for the samples with $0.12 < x < 0.16$, we note that there are drops to zero in resistivity data, but there is no accompanying specific-heat anomaly, indicating filamentary superconductivity.

Several physical quantities of $\text{Ge}_{1-x}\text{In}_x\text{Te}$ are summarized in Fig. 3. The evolution of the unit-cell volume with x is shown in Fig. 3(a). As summarized in Section S2 of the

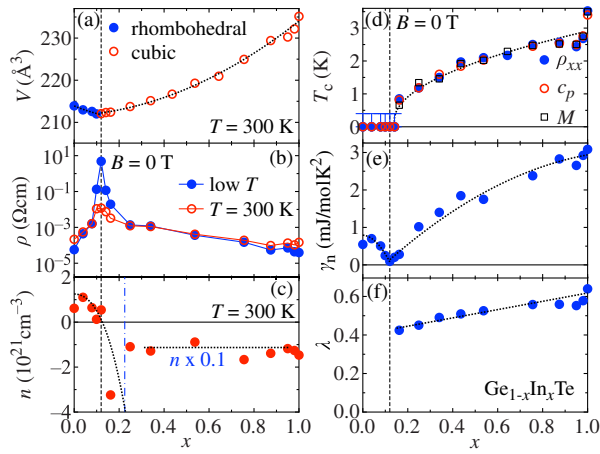


FIG. 3. Variation of physical quantities in $\text{Ge}_{1-x}\text{In}_x\text{Te}$. (a) Pseudocubic unit-cell volume for rhombohedral ($x < 0.12$) and cubic structure ($x > 0.12$) at 300 K. (b) Zero-field resistivity at 300 K (red open symbols) and at low T (blue filled symbols; at 2 K for $x \leq 0.25$ and above T_c for larger x). (c) Charge-carrier concentration n at 300 K. Note that n for $x \geq 0.25$ (dashed-dotted vertical line) are multiplied by 0.1 for clarity. (d) Superconducting T_c as estimated from resistivity, specific heat, and magnetization. The error bars for data points below $x = 0.16$ indicate that these samples do not superconduct down to approx. 400 mK. (e) Normal-state electronic specific-heat coefficients γ_n . (f) Electron-phonon coupling strength deduced from specific-heat data. Dotted lines are guides to the eyes, solid horizontal lines in (c)–(e) indicate baselines, and the dashed vertical lines denote $x_c = 0.12$.

SM [14], there is a coexistence region $0.08 \leq x < 0.14$ with rhombohedral and cubic phase fractions, and the structure is better described in rhombohedral for $x < 0.12$ and in cubic above. Interestingly, the unit-cell volume V shrinks as long as the system is rhombohedrally distorted while V strongly increases in the cubic phase. Notably, Vegard's law is violated: the slope of $V(x)$ starts to increase above $x \sim 0.25$. The lattice constants are shown in Fig. S3(a) of the SM [14].

Absolute values of ρ_{xx} at 300 K and at low T (at 2 K for $x \leq 0.25$ and above T_c for larger x) are plotted against x in Fig. 3(b). The sharp and strong enhancement of ρ_{xx} around $x_c = 0.12$ is most pronounced at low T and still clearly recognized at 300 K, highlighting this critical In-doping concentration.

In Fig. 3(c), the charge-carrier concentrations n are plotted against x as estimated from magnetic field B dependent Hall effect $\rho_{yx}(B)$ measurements at 300 K, although n deduced from $\rho_{yx}(B)$ may show some deviation from the real value for metallic samples. The hole-type charge-carrier concentration is quickly suppressed when introducing In, and changes sign around $x_c = 0.12$, i.e., the most insulating doping range. In spite of the semiconductorlike slope of $\rho_{xx}(T)$ for $0.25 \leq x < 0.44$, the electron concentrations in these samples are already of the order of 10^{22} cm^{-3} , and hence, the conduction regime is barely metallic. For $x > 0.44$, n stays almost constant around

10^{22} cm^{-3} . The cation deficiency δ , which may affect n , is described in Section S6 of the SM [14].

Superconducting T_c values as estimated from resistivity, specific-heat, and magnetization data increase monotonically with x and agree well with each other, see Fig. 3(d). Notably, near InTe, T_c increases very rapidly.

Figure 3(e) shows the evolution of γ_n with x . The γ_n value of the measured GeTe sample has a smaller value than the sample for $x = 0.04$, probably due to the particular value of the Ge deficiency of the examined specimen. Upon increasing x , γ_n is reduced and almost zero but finite around $x_c = 0.12$ in accord with the charge-carrier concentration. For larger x , γ_n increases monotonously.

Figure 3(f) summarizes the electron-phonon coupling strength λ as estimated from specific-heat analyses. It increases with almost constant slope over the superconducting doping range $0.16 \leq x \leq 1$. The strong enhancement of T_c for $x = 1$ is neither clearly reflected in γ_n nor in λ , cf. Section S9 of the SM [14].

To obtain information on how the electronic structure changes upon In doping, we performed photoemission spectroscopy. Figure 4(a) shows the valence-band spectra for $x \leq 0.25$ around E_F , which is indicated by a vertical solid line. The observed behavior is typical for a p -type semiconducting system. Arrows indicate the valence-band maximum (VBM). The energy values of the VBM are replotted in Fig. 4(b). Apparently, the VBM shifts linearly with x from above to below E_F and coincides with E_F at $x_c = 0.12$, indicating the depletion of the charge carriers at and their sign change across x_c . At higher $x \geq 0.44$, the spectra change qualitatively from semiconducting to metallic as seen in Figs. S6(a) and S6(b) of the SM [14]. A step or edge at E_F reflects the metallic character of these samples.

Bulk-sensitive x-ray PES measurements ($h\nu = 1486.6 \text{ eV}$) for the In- $3d_{5/2}$ core level allowed us to obtain information about the valence state of In, cf. Fig. S6(c) of the SM [14]. In the intermediate doping region $0.25 < x < 0.64$, the core-level structure broadens, and the peak position changes suddenly around $x = 0.34$. The peak energies are replotted in Fig. 4(c). These two values are associated with the two valence states of In. Dashed horizontal lines are guides for the energies of both features. They are separated by approximately 0.2 eV, similarly as Sn^{2+} and Sn^{4+} peaks in Sn core-level spectra of AgSnSe_2 [11] or Sn oxides [53]. In the case of AgSnSe_2 , Sn^{2+} and Sn^{4+} peaks appear at binding energies of ~ 485.6 and ~ 486.3 eV, respectively, thus, indicating a separation of ~ 0.7 eV. In analogy with this behavior, we attribute the energetically shallower feature (~ 444.25 eV) to the In^{1+} and the deeper one (~ 444.44 eV) to the In^{3+} state.

Given the observed superconductor-semiconductor-superconductor transition induced by valence-skipping In with favorable In^{1+} ($4d^{10}5s^2$) and In^{3+} ($4d^{10}5s^0$) valence states [5,7,54], we will finally discuss their role based on the sketch in Fig. 4(d). It illustrates the plausible evolution of the In states as a function of x on the basis of the results

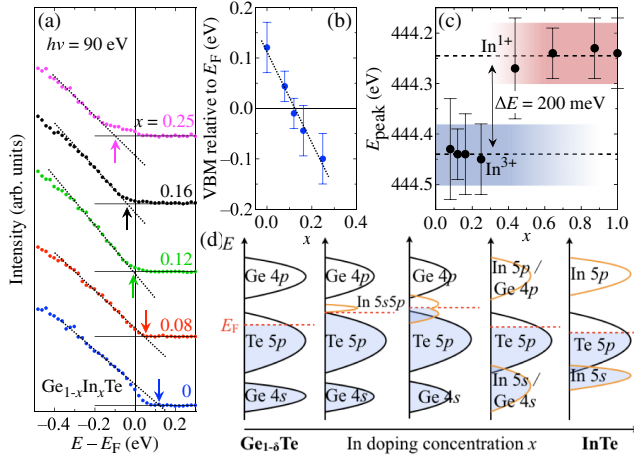


FIG. 4. (a) Valence-band photoemission spectra of $\text{Ge}_{1-x}\text{In}_x\text{Te}$ for $x \leq 0.25$ recorded by the photon energy of $h\nu = 90$ eV. Data for different x are shifted with respect to each other for clarity. The vertical solid line represents E_F . At each data set, horizontal solid lines indicate the baseline and dotted lines are linear fits to the data below E_F . The arrows denote the energies where these lines intersect as a measure of the VBM energy. (b) Replotted VBM energies as a function of x . The sign change indicates where E_F shifts above the VBM, coinciding with $x_c = 0.12$. The dotted line is a guide to the eyes. (c) Peak energies of In- $3d_{5/2}$ -core-level photoemission spectra are plotted against x , demonstrating the two different In-valence states. Gradations indicate the coexistence region of both valence states, and the change from mainly In^{3+} (blue; low doping) to mainly In^{1+} (red; high doping). Dashed horizontal lines indicate the average peak energy of each feature which differ by approximately 200 meV. (d) Schematic illustration of the evolution of the band structure [46] in $\text{Ge}_{1-x}\text{In}_x\text{Te}$ with x , see text.

summarized in Figs. 1–4. The left-most schematic DOS shows the situation in $\text{Ge}_{1-\delta}\text{Te}$. The Fermi level lies in the Te- $5p$ band, giving rise to metalliclike conduction with hole-type carriers. The second picture shows the situation for light In doping, which effectively reduces the hole-type carriers, shifting E_F upwards. According to Ref. [2], light In doping leads to the formation of impurity states located at the top of the VBM. This is also confirmed by our band calculation for $x_c = 0.12$ (Section S10 in the SM [14]). In the sketch, this feature is labelled “In $5s5p$ ” to emphasize its origin from the respective atomic In orbitals. These newly formed states are mostly empty, and hence, the initial valence state of In is $3+$.

Upon further doping, the impurity band becomes wider and the initial In $5s5p$ states start to separate as shown in the central drawing of Fig. 4(d). The conduction mechanism will gain again metallic character above $x_c = 0.12$. Recently, the bonding state in GeTe is discussed as incipient metal due to a competition between localization and delocalization [55–57]. If this holds for light In doping, one might speculate whether this type of bonding helps facilitating the superconductivity in $\text{Ge}_{1-x}\text{In}_x\text{Te}$ as soon as

the In doping drives the system into a conducting regime again, i.e., for $x > 0.12$. The next schematic shows how the bands of In $5p - \text{Ge } 4p$ and In $5s - \text{Ge } 4s$ characters form mixed orbital states at higher doping, called “amalgamated bands” in Ref. [58]. When the doping level is sufficiently high, the In- $5s$ orbitals will have developed into a proper fully occupied band below E_F . Only the In- $5p$ band remains empty, thus, In now takes its $1+$ state.

The analysis of the In- $3d_{5/2}$ core-level photoemission spectra yields further confirmation: For low doping up to $x \sim 0.25$, we can only identify the feature at higher binding energy (In^{3+}). From $x = 0.25$ a second feature develops, indicating that the valence state of the dopants starts to become $1+$. At the same time, the peak representing the In^{3+} state fades away and is hardly seen for $x > 0.44$, cf. Fig. S6(c) of the SM [14]. Therefore, the crossover from $3+$ to $1+$ mainly takes place between $x \sim 0.25$ and ~ 0.64 , cf. Fig. 4(c). Nevertheless, it is likely that some In dopants start to take their $1+$ state already around $x_c \approx 0.12$ and, hence, leading to the formation of additional DOS as indicated by the monotonic increase of γ_n for $x > 0.12$, cf. Fig. 3(e). When $\text{Ge}_{1-x}\text{In}_x\text{Te}$ has completely switched to cubic structure and sufficient DOS has formed at E_F , superconductivity appears, i.e., at a slightly higher $x > x_c$. Hence, the emergence of superconductivity is related to the valence instability of the In dopant. The increasing number of In^{1+} dopants further enhances the superconductivity by providing more and more DOS, which explains why T_c , γ_n , and λ [cf. Figs. 3(d)–3(f)] increase monotonically with x . The valence change is also reflected in the nonmonotonic behavior of the unit-cell volume V with x , cf. Fig. 3(a): V decreases as x increases to $x_c = 0.12$ because of the smaller ionic radius of In^{3+} , but tends to nonlinearly increase above x_c due to the increasing fraction of larger In^{1+} ions.

At higher doping, the system behaves like a metal as indicated by resistivity data [Fig. 1(e)]. This situation is sketched in the final drawing in Fig. 4(d) for pure InTe, where a metallic ground state with a large Fermi surface and empty In- $5p$ bands is realized. To assume the $1+$ state for In is reasonable even for metallic InTe, because of the energetic proximity of the Te $5p$ and In $5p$ states allowing an easy charge transfer.

In summary, we report the discovery of a superconductor-semiconductor-superconductor transition in $\text{Ge}_{1-x}\text{In}_x\text{Te}$ and the existence of a critical doping concentration $x_c = 0.12$, where various properties are governed or strongly affected by the crossover of the In valence state from $3+$ to $1+$: The structure changes from polarly rhombohedral to cubic, the resistivity increases by orders of magnitude, the charge-carrier type changes from holes to electrons, and the density of states diminishes at the dawn of an emerging superconducting phase. This highlights the question about the exact role of the associated valence instability in superconducting systems such as In-doped GeTe and SnTe, which is a promising starting point for future studies.

This work was partly supported by Grants-In-Aid for Scientific Research (S) from the Japan Society for the Promotion of Science (JSPS, No. 24224009), JST (No. JP16H00924), CREST JST (No. JPMJCR16F1), and PRESTO (No. JPMJPR15N5), Grant-In-Aid for Scientific Research (B) (JSPS, No. 17H02770), and Grant-In-Aid for Scientific Research (C) (JSPS, No. 15K05140). We thank R. Arita and T. Koretsune for fruitful discussions.

*Corresponding author.

markus.kriener@riken.jp

- [1] M. Cohen, *Phys. Rev.* **134**, A511 (1964).
- [2] N. Haldolaarachchige, Q. Gibson, W. Xie, M. B. Nielsen, S. Kushwaha, and R. J. Cava, *Phys. Rev. B* **93**, 024520 (2016).
- [3] K. Kobayashi, Y. Ai, H. O. Jeschke, and J. Akimitsu, *Phys. Rev. B* **97**, 104511 (2018).
- [4] M. Kriener, M. Kamitani, T. Koretsune, R. Arita, Y. Taguchi, and Y. Tokura, *Phys. Rev. Mater.* **2**, 044802 (2018).
- [5] C. Varma, *Phys. Rev. Lett.* **61**, 2713 (1988).
- [6] M. Dzero and J. Schmalian, *Phys. Rev. Lett.* **94**, 157003 (2005).
- [7] I. Hase, K. Yasutomi, T. Yanagisawa, K. Odagiri, and T. Nishio, *Physica (Amsterdam)* **527C**, 85 (2016).
- [8] I. Hase, T. Yanagisawa, and K. Kawashima, *Nanoscale Res. Lett.* **12**, 127 (2017).
- [9] Y. Matsushita, H. Bluhm, T. H. Geballe, and I. R. Fisher, *Phys. Rev. Lett.* **94**, 157002 (2005).
- [10] Z. Ren, M. Kriener, A. A. Taskin, S. Sasaki, K. Segawa, and Y. Ando, *Phys. Rev. B* **87**, 064512 (2013).
- [11] T. Wakita, E. Paris, K. Kobayashi, K. Terashima, M. Y. Hacısalıhođlu, T. Ueno, F. Bondino, E. Magnano, I. Piř, L. Olivi *et al.*, *Phys. Chem. Chem. Phys.* **19**, 26672 (2017).
- [12] R. J. Cava, B. Batlogg, J. J. Krajewski, R. Farrow, L. W. Rupp, Jr., A. E. White, K. Short, W. F. Peck, and T. Kometani, *Nature (London)* **332**, 814 (1988).
- [13] A brief comparison of $\text{Sn}_{1-x}\text{In}_x\text{Te}$ and $\text{Ge}_{1-x}\text{In}_x\text{Te}$ can be found in Section S11 of the Supplemental Material Ref. [14].
- [14] See Supplemental Material at <http://link.aps.org/supplemental/10.1103/PhysRevLett.124.047002> for complementing data which includes Refs. [15–28].
- [15] K. Momma and F. Izumi, *J. Appl. Crystallogr.* **44**, 1272 (2011).
- [16] P. Blaha, K. Schwarz, G. K. H. Madsen, D. Kvasnicka, J. Luitz, R. Laskowski, F. Tran, and L. D. Marks, WIEN2k Package, Version 13.1. Techn. Universität Wien, Austria (2013).
- [17] M. D. Banus, R. E. Hanneman, M. Stroncin, and K. Goen, *Science* **142**, 662 (1963).
- [18] H. E. Bömmel, A. J. Darnell, W. F. Libby, B. R. Tittmann, and A. J. Yencha, *Science* **141**, 714 (1963).
- [19] S. Geller, A. Jayaraman, and G. W. Hull, Jr., *Appl. Phys. Lett.* **4**, 35 (1964).
- [20] S. Geller and G. W. Hull, Jr., *Phys. Rev. Lett.* **13**, 127 (1964).
- [21] J. K. Hulm, M. Ashkin, D. W. Deis, and C. K. Jones, *Prog. Low Temp. Phys.* **6**, 205 (1970).
- [22] E. H. Brandt, *Phys. Rev. B* **60**, 11939 (1999).
- [23] M. P. Seah and W. A. Dench, *Surf. Interface Anal.* **1**, 2 (1979).
- [24] M. Novak, S. Sasaki, M. Kriener, K. Segawa, and Y. Ando, *Phys. Rev. B* **88**, 140502(R) (2013).
- [25] S. Sasaki, Z. Ren, A. A. Taskin, K. Segawa, L. Fu, and Y. Ando, *Phys. Rev. Lett.* **109**, 217004 (2012).
- [26] S. Maeda, R. Hirose, K. Matano, M. Novak, Y. Ando, and G.-q. Zheng, *Phys. Rev. B* **96**, 104502 (2017).
- [27] Y. Tanaka, Z. Ren, T. Sato, K. Nakayama, S. Souma, T. Takahashi, K. Segawa, and Y. Ando, *Nat. Phys.* **8**, 800 (2012).
- [28] T. Sato, Y. Tanaka, K. Nakayama, S. Souma, T. Takahashi, S. Sasaki, Z. Ren, A. A. Taskin, K. Segawa, and Y. Ando, *Phys. Rev. Lett.* **110**, 206804 (2013).
- [29] J. E. Boschker, R. Wang, and R. Calarco, *Cryst. Eng. Commun.* **19**, 5324 (2017).
- [30] R. Hein, J. Gibson, R. Mazelsky, R. Miller, and J. Hulm, *Phys. Rev. Lett.* **12**, 320 (1964).
- [31] D. Lencer, M. Salinga, B. Grabowski, T. Hickel, J. Neugebauer, and M. Wuttig, *Nat. Mater.* **7**, 972 (2008).
- [32] M. Kriener, T. Nakajima, Y. Kaneko, A. Kikkawa, X. Z. Yu, N. Endo, K. Kato, M. Takata, T. Arima, Y. Tokura *et al.*, *Sci. Rep.* **6**, 25748 (2016).
- [33] M. Kriener, T. Nakajima, Y. Kaneko, A. Kikkawa, D. Hashizume, K. Kato, M. Takata, T. Arima, Y. Tokura, and Y. Taguchi, *Phys. Rev. B* **95**, 224418 (2017).
- [34] R. W. Cochrane, M. Plischke, and J. O. Ström-Olsen, *Phys. Rev. B* **9**, 3013 (1974).
- [35] H. Przybylińska, G. Springholz, R. T. Lechner, M. Hassan, M. Wegscheider, W. Jantsch, and G. Bauer, *Phys. Rev. Lett.* **112**, 047202 (2014).
- [36] D. Kriegner, J. Furthmüller, R. Kirchschrager, J. Endres, L. Horak, P. Cejpek, H. Reichlova, X. Marti, D. Primetzhofer, A. Ney *et al.*, *Phys. Rev. B* **94**, 054112 (2016).
- [37] E. M. Levin, M. F. Besser, and R. Hanus, *J. Appl. Phys.* **114**, 083713 (2013).
- [38] F. Herman, R. L. Kortum, I. B. Ortenburger, and J. P. van Dyke, *J. Phys. (Paris), Colloq.* **29**, C4-62 (1968).
- [39] A. Lau and C. Ortix, *Phys. Rev. Lett.* **122**, 186801 (2019).
- [40] D. D. Sante, P. Barone, R. Bertacco, and S. Picozzi, *Adv. Mater.* **25**, 509 (2013).
- [41] J. Krempaský, S. Muff, F. Bisti, M. Fanciulli, H. Volfová, A. Weber, N. Pilet, P. Warnicke, H. Ebert, J. Braun *et al.*, *Nat. Commun.* **7**, 13071 (2016).
- [42] We note that, in literature, the ferroelectric distortion is traced back to either a displacive or an order-disorder transition, cf. Refs. [43,44], and references therein.
- [43] P. Fons, A. V. Kolobov, M. Krbal, J. Tominaga, K. S. Andrikopoulos, S. N. Yannopoulos, G. A. Voyiatzis, and T. Uruga, *Phys. Rev. B* **82**, 155209 (2010).
- [44] T. Matsunaga, P. Fons, A. V. Kolobov, J. Tominaga, and N. Yamada, *Appl. Phys. Lett.* **99**, 231907 (2011).
- [45] J. Goldak, C. S. Barrett, D. Innes, and W. Youdelis, *J. Chem. Phys.* **44**, 3323 (1966).
- [46] We note that the density of states below E_F consists not purely of Te $5p$ states, but also contains some contributions originating from Ge states. For simplicity they are omitted in Figs. 1(c) and 4(d).
- [47] For a comprehensive discussion of the Ge vacancy formation, see A. H. Edwards, A. Pineda, P. Schultz, M. Martin,

- A. Thompson, H. Hjalmarson, and C. Umrigar, *Phys. Rev. B* **73**, 045210 (2006).
- [48] J. C. Woolley, *J. Electrochem. Soc.* **112**, 906 (1965).
- [49] N. K. Abrikosov and G. T. Danilova-Dobryakova, *Intermetallics* **12**, 1005 (1976).
- [50] S. A. Némov, R. V. Parfeniev, D. V. Shamshur, M. O. Safonchik, and J. Stepien-Damm, *Czech. J. Phys.* **46**, 863 (1996).
- [51] L. Wu, X. Li, S. Wang, T. Zhang, J. Yang, W. Zhang, L. Chen, and J. Yang, *NPG Asia Mater.* **9**, e343 (2017).
- [52] The charge carrier concentration of the sample $\text{Ge}_{1-\delta}\text{Te}$ used in this study suggests that it does not superconduct down to 50 mK according to the phase diagram published in Ref. [30].
- [53] J.-M. Themlin, M. Chtaib, L. Henrard, P. Lambin, J. Darville, and J.-M. Gilles, *Phys. Rev. B* **46**, 2460 (1992).
- [54] A. S. Erickson, J.-H. Chu, M. F. Toney, T. H. Geballe, and I. R. Fisher, *Phys. Rev. B* **79**, 024520 (2009).
- [55] M. Zhu, O. Cojocaru-Mirédin, A. M. Mio, J. Keutgen, M. Küpers, Y. Yu, J. Cho, R. Dronskowski, and M. Wuttig, *Adv. Mater.* **30**, 1706735 (2018).
- [56] M. Wuttig, V.L. Deringer, X. Gonze, C. Bichara, and J. Raty, *Adv. Mater.* **30**, 1803777 (2018).
- [57] J. Raty, M. Schumacher, P. Golub, V.L. Deringer, C. Gatti, and M. Wuttig, *Adv. Mater.* **31**, 1806280 (2019).
- [58] Y. Onodera and Y. Toyozawa, *J. Phys. Soc. Jpn.* **24**, 341 (1968).